Optics Letters

Dielectric perturbations: anomalous resonance frequency shifts in optical resonators

Farhan Azeem,[1,2] Luke S. Trainor,[1,2] Patrick A. Devane,[1,2] Daniel S. Norman,[1,2] Alfredo Rueda,[1,2] Nicholas J. Lambert,[1,2] Madhuri Kumari,[1,2] Matthew R. Foreman,[3] and Harald G. L. Schwefel[1,2,*]

[1]The Dodd-Walls Centre for Photonic and Quantum Technologies, New Zealand
[2]Department of Physics, University of Otago, 730 Cumberland Street, Dunedin 9016, New Zealand
[3]Blackett Laboratory, Department of Physics, Imperial College London, Prince Consort Road, London SW7 2AZ, UK
*Corresponding author: harald.schwefel@otago.ac.nz

Received 5 February 2021; revised 2 April 2021; accepted 8 April 2021; posted 8 April 2021 (Doc. ID 420791); published 12 May 2021

Small perturbations in the dielectric environment around resonant dielectric structures usually lead to a frequency shift of the resonator modes directly proportional to the polarizability of the perturbation. Here, we report experimental observations of strong frequency shifts that can oppose and even exceed the contribution of the perturbations' polarizability. We show in particular how the mode frequencies of a lithium niobate whispering-gallery-mode resonator are shifted by planar substrates—of refractive indices ranging from 1.50 to 4.22—contacting the resonator rim. Both blue- and redshifts are observed, as well as an increase in mode linewidth, when substrates are moved into the evanescent field of the whispering gallery mode. We compare the experimental results to a theoretical model by Foreman *et al*. [J. Opt. Soc. Am. B 33, 2177 (2016)] and provide an additional intuitive explanation based on the Goos–Hänchen shift for the optical domain, with applications to dielectric structures ranging from meta-surfaces to photonic crystal cavities.

https://doi.org/10.1364/OL.420791

Small perturbations are at the core of many branches of physics. The textbook description of a small perturbation in the permittivity or permeability within an electromagnetic resonant system leads to the Bethe–Schwinger perturbation theory [1]. One of its most straightforward applications is to the case of a dielectric microresonator perturbed by a contribution to the dielectric environment for which it predicts a small shift of the resonance frequency. If the perturbation is small enough it was assumed that the dipole approximation was valid, whereby the complex frequency shift is related to the polarizability and hence results in a redshift of the resonance frequency. This view was particularly fruitful in considering optical microresonators for sensing of refractive index [2,3], nanoparticles [4–7] such as viruses [8], bacteria [9], single molecules [8] and proteins [10,11], as well as in thermal sensing [12]. Recently, however, more in-depth studies have shown that small perturbations can have much more complex results, i.e., both red- and blueshifts of the resonance frequency are possible [13,14]. The key factor herein is that in an open system, the radiative contributions of the perturbation—besides the mode broadening [15]—need to be taken into account as well. This has led to the experimental discovery of strong blueshifts in the perturbation of a small toroidal resonator with plasmonic antennas [14].

Another prediction of this theory is that such shifts also exist when a dielectric interface is introduced into the vicinity of a dielectric whispering-gallery-mode (WGM) resonator [13]. Optical WGM resonators are based on the principle of total internal reflection (TIR) of light along the internal boundary of a transparent dielectric [16]. In low loss materials, quality (Q) factors of over one hundred million have readily been achieved in varying geometries [17,18], leading to applications in optical sensing [19,20], and when an optically non-linear material is used [21], resulting in generation of frequency combs [22,23]. An extended list of applications of WGM resonators also includes non-linear photonics [24,25], quantum optics [16,26–28], microwave to optical conversion [29–31], optical communication [32–34], electro-optical modulation [35], and lasers [36].

The effect of dielectric perturbations has already been used to carefully phase-match parametric down conversion in lithium niobate WGM resonators [37]. Various other methods are also employed to shift the resonance position in WGM resonators, including exploiting the thermo-optical [38,39] and electro-optical effects [40], as well as deforming the resonator by external strain [41,42].

Frequency tuning of WGMs by perturbing the dielectric environment has been studied analytically [13] for a disk-shaped lithium niobate ($LiNbO_3$) resonator. The results of this study show mode broadening in both the transverse electric (TE) and transverse magnetic (TM) polarized modes. The TM-polarized modes exhibit only a redshift in frequency for the given range of refractive indices studied, whereas the TE-polarized modes exhibit both a redshift and an anomalous blueshift. Moreover, an anomalous blueshift in the mode frequency of a toroid-shaped silica resonator has been demonstrated experimentally [14], via gold nano-antennas deposited

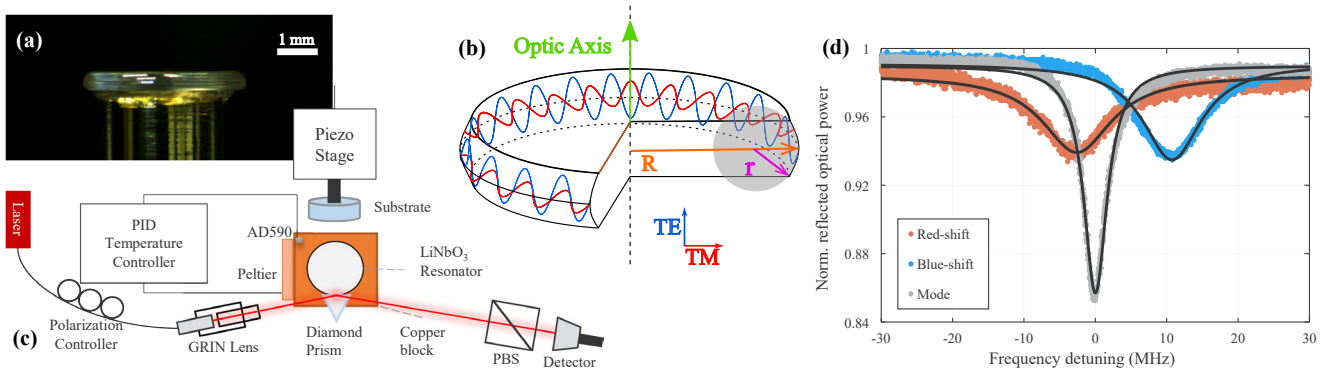

Fig. 1. Configuration of the experiment. (a) $LiNbO_3$ WGM resonator. (b) Schematic of the WGM showing the optic axis, polarization of the modes, radius of the disk (R), and radius of curvature of the resonator (r). (c) Schematic of the experimental setup to observe the effect of planar dielectric substrates on the WGMs of $LiNbO_3$ resonator. A telecom laser is evanescently coupled using a diamond prism into a temperature-stabilized resonator. The input polarization is controlled, and sidebands can be modulated onto the laser for calibration. Both the prism and the dielectric substrate are moved using piezo positioners with nanometer precision. (d) Normalized reflected optical power versus frequency. The high Q TE mode is shown in gray. The redshift due to the $LiNbO_3$ substrate is shown in red, whereas the blueshift due to the introduction of Ge substrate within the resonator's evanescent field is shown in blue. Mode broadening is also observed in both instances. The coupling efficiency is reduced by more than 50% in both cases, which is attributed mainly to the additional out-coupling losses induced by the presence of the substrate.

on a glass substrate. Furthermore, blueshifts have been experimentally demonstrated in a silicon sphere WGM resonator in the terahertz (THz) domain [43].

Here, for the first time, we show experimental results confirming the prediction in Ref. [13], in the optical domain. The frequency shifts and broadening of the mode are observed for both TE and TM polarizations. An anomalous blueshift is observed for TE polarization, when substrates of higher refractive indices are brought into close proximity to the resonator. We also compare the results to an intuitive explanation based on the Goos–Hänchen shift.

At the core of the experiment is a disk-shaped z-cut $LiNbO_3$ WGM resonator ($n_o = 2.21$, $n_e = 2.14$ [44]), shown in Fig. 1(a). The symmetry of the resonator is shown in Fig. 1(b). The resonator has a major radius $R = 2$ mm and a minor radius $r = 0.23$ mm, and modes with either TE or TM polarization can be excited. The schematic of the experiment is shown in Fig. 1(c). A fiber-coupled tunable diode laser (DL) with a central wavelength of 1550 nm is the excitation source for the WGMs. The output from the DL is fed to a phase modulator (PM) to modulate sidebands onto the input laser signal for accurate frequency calibration of the DL scan range. A frequency scan of the laser reveals the reflection spectrum of the WGMs. TE and TM modes are selected using a polarization controller. A diamond prism ($n_p = 2.38$ [45]) is used to couple into the temperature stabilized resonator, with the laser output from the fiber focused onto the prism–resonator interface using a graded-index (GRIN) lens. The output light from the resonator is passed through a polarizing beam splitter (PBS) to select the desired polarization. The light is then collected by an indium gallium arsenide photodiode, and the output digitized using an oscilloscope.

A piezo stage moves the substrates into close proximity to the WGM resonator with nanometer accuracy. Seven substrates (listed in Table S1 of Supplement 1) of varying refractive indices (n_{sub}) [44,46–52] are used. The substrate is slowly moved towards the resonator until they are in contact, with a spectrum recorded at each step. Lorentzian fits are applied to the acquired spectra to extract the linewidths and the frequency positions of the mode. Throughout the measurements, we took particular care to track a single high Q mode from each polarization, even while interchanging substrates.

As soon as the substrate penetrates a significant proportion of the evanescent field of the mode, a shift in the resonance frequency and mode broadening are observed. Example red- and blueshifts of the TE mode are plotted in Fig. 1(d). If the refractive index of the substrate is higher than that of the resonator ($n_{sub} > n_{res}$), the linewidth of the mode increases as the substrate approaches the resonator. Moreover, a decrease or an increase in the resonance frequency is observed, depending on the type of substrate and polarization. The coupling efficiency to the mode changes as the distance between the resonator and the substrate decreases; additional losses (mode broadening) due to the substrate increase the system's total loss rate, whereas the coupling rate to the diamond prism remains the same. This combination changes the coupling regime. In Fig. 1(d), the depths of the resonances decrease when the substrates are introduced as the mode becomes significantly under-coupled.

To quantify the mode broadening and frequency shift, we repeated the approach of each dielectric substrate to the resonator multiple times. In the data for each approach, the linewidth contains a constant term (due to intrinsic resonator losses as well as the coupling rate to the diamond prism) as well as a term that increases exponentially as the distance between the resonator and substrate decreases due to the increasing piezo voltage. Beyond a particular piezo voltage, the linewidth growth is no longer exponential. We attribute this piezo voltage to be the voltage at which the resonator and prism touch, and further increase of piezo voltage serves only to move or squash the rim of the resonator slightly. From an exponential fit to the linewidth, we extract the mode broadening due to the substrate at this touching voltage. The resonance frequency also changes with an exponential distance dependence upon approach of the substrate. A constant linear drift of the resonance frequency for each approach was removed, as it was attributed to slow thermal heating/cooling of the device. After removal, the resonance frequency shift was fitted to an exponential, and the value at the touching point (as determined from the linewidth data)

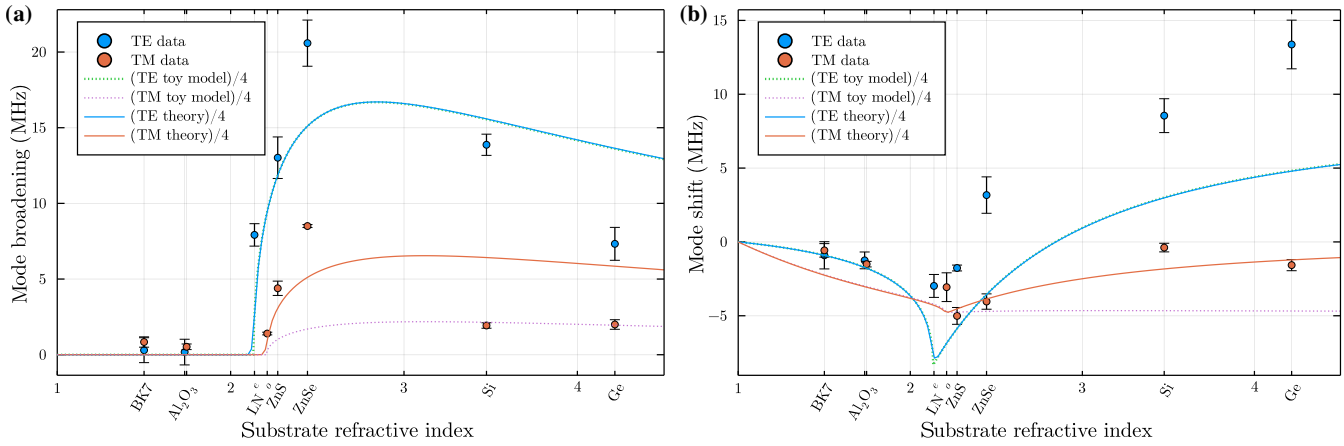

Fig. 2. (a) Linewidth broadening and (b) resonance frequency shift in TE and TM modes versus the substrate refractive index. Dots are the measured values, and their error bars correspond to the 95% confidence interval deduced from repeated measurements. Solid curves depict the analytical theory of Foreman *et al*. [13] and dotted curves the toy model, each of which has been scaled by a phenomenological factor of 1/4.

was recorded. The final results from different runs of the same substrate were averaged. An example of the dependence of mode broadening and resonance frequency shift on distance is shown in Fig. S1 in Supplement 1.

The increase in the linewidth of the mode due to dielectrics of different refractive indices is shown in Fig. 2(a), whereas Fig. 2(b) shows the shift in the resonance frequency of the mode. The TM-polarized mode exhibits only redshifts. However, the TE-polarized mode shows both redshifts and blueshifts, depending on the substrate's refractive index. Dielectric substrates with refractive indices significantly larger than that of the resonator excite an anomalous blueshift. A blueshift as high as 14 MHz is observed for TE polarization, whereas a redshift as low as −5 MHz is observed for TM polarization. The strongest redshifts are seen when using the ZnS substrate for the TM-polarized mode, and the $LiNbO_3$ substrate for the TE-polarized mode.

Our results are in qualitative agreement with the theory described by Foreman *et al*. [13]. However, the model predicts both frequency shifts and mode broadening to be approximately a factor of four larger than those observed. We ascribe this discrepancy to experimental deviations from the ideal situation. In particular, the relevant surfaces of the substrates used to tune the resonances are unlikely to be completely parallel to the symmetry axis of the resonator. This leads to a small air gap between the resonator and substrate at the equator of the WGM, which reduces the magnitude of the effects due to the substrate. As an example, a small angle of 2° would lead to an air gap of 140 nm; this is comparable to the evanescent decay length of approximately 130 nm.

A simple toy model based on an altered Goos–Hänchen shift at the resonator rim can explain the shape of the expected resonance shifts, as the effective perimeter of the resonator shifts in or out. When light undergoes TIR, it appears to shift laterally, a phenomenon termed the Goos–Hänchen shift [53,54], which has been successfully used in the analysis of deformed microresonators [55]. The reason is that the Fresnel reflection coefficient for TIR has an extra phase shift, $r_0 = -\exp(-i\Theta)$, such that the light appears to reflect off a surface that is a distance of $\delta R = \Theta/(2k_0 n_{\mathrm{res}} \cos\theta_i)$ away from the real surface [56,57], where k_0 is the vacuum wavevector of the light, n_{res} is the bulk refractive index of the resonator, and θ_i is the angle of incidence of the light on the boundary. When we introduce a dielectric close to the resonator, we alter the phase of the reflection coefficient (and if the light can tunnel out into that dielectric, we alter its magnitude). We therefore alter the effective radius of the resonator in the region of the dielectric.

To show that an altered effective boundary explains the resonance shifts, we evaluate the reflection coefficient if we introduce a dielectric at a small (constant) effective distance d_{eff} away from the resonator. We separate the new reflection coefficient into the terms $r = -\exp(-i(\Theta + \delta\Theta) - \alpha)$, where $\delta\Theta \in \mathbb{R}$ is the additional phase-shift due to the substrate, which causes a resonance frequency shift. $\alpha \geq 0$ is a loss factor due to tunneling of the light into the outer substrate, which causes mode broadening. $\delta\Theta$ and α both depend on d_{eff} and the refractive indices. The reflection coefficients were calculated using the tmm Python package [58]. Using the effective distance between the resonator and the dielectric as a fitting parameter, we find remarkable agreement to the theory with $d_{\mathrm{eff,TE}} = 438.4$ nm for TE polarization for all substrate refractive indices, and $d_{\mathrm{eff,TM}} = 352.8$ nm for TM polarization, albeit only when the substrate refractive index is less than the resonator refractive index. The predicted values are plotted as dotted lines in Fig. 2. A depiction of the Goos–Hänchen shift in the case of our WGM resonator and dielectric substrates is shown in Fig. S2 in Supplement 1. It shows how the resonance shift is effected by the mode being "pushed into" or "pulled out of" the resonator in the vicinity of the dielectric.

In conclusion, we have observed frequency shifts and mode broadening due to the introduction of dielectric materials into the evanescent field. Remarkably, both blue- and redshifts were observed. Our results agree qualitatively with the theory in Ref. [13]. The type of shift in frequency also depends on the polarization of the excited mode; the TM-polarized mode is only redshifted, whereas the TE-polarized mode is both redshifted and blueshifted. Substrates of higher refractive indices such as Ge, Si, and ZnSe excite a blueshift in TE polarization. An anomalous blueshift as high as 14 MHz due to the Ge substrate is observed. Conversely, the largest redshift recorded is −5 MHz, when a $LiNbO_3$ substrate is used to tune the mode. For the particular case of WGM resonators, these results have

implications for effective mode tuning without the application of any external strain, which can aid in achieving optimum phase-matching conditions for non-linear processes. More generally, they show that the interplay between dispersive and dissipative components and the real and imaginary parts of the electromagnetic fields can yield initially non-intuitive results, just as for perturbed photonic crystal cavities [59], or more generally non-Hermitian photonics [60–63].

Funding. Ministry of Business, Innovation and Employment (UOOX1805); Marsden Fund (17-UOO-002); Royal Society (UF150335).

Acknowledgment. We acknowledge fruitful discussions with Florian Sedlmeir.

Disclosures. The authors declare no conflicts of interest.

Data Availability. Data underlying the results presented in this paper are not publicly available at this time but may be obtained from the authors upon reasonable request.

Supplemental document. See Supplement 1 for supporting content.

REFERENCES

1. R. Waldron, Proc. IEE Part C Monographs **107**, 272 (1960).
2. I. Teraoka, S. Arnold, and F. Vollmer, J. Opt. Soc. Am. B **20**, 1937 (2003).
3. Y.-F. Xiao, V. Gaddam, and L. Yang, Opt. Express **16**, 12538 (2008).
4. S. Arnold, D. Keng, S. I. Shopova, S. Holler, W. Zurawsky, and F. Vollmer, Opt. Express **17**, 6230 (2009).
5. M. Baaske and F. Vollmer, Chem. Phys. **13**, 427 (2012).
6. L. Shao, X.-F. Jiang, X.-C. Yu, B.-B. Li, W. R. Clements, F. Vollmer, W. Wang, Y.-F. Xiao, and Q. Gong, Adv. Mater. **25**, 5616 (2013).
7. B.-Q. Shen, X.-C. Yu, Y. Zhi, L. Wang, D. Kim, Q. Gong, and Y.-F. Xiao, Phys. Rev. Appl. **5**, 024011 (2016).
8. F. Vollmer, S. Arnold, and D. Keng, Proc. Natl. Acad. Sci. USA **105**, 20701 (2008).
9. H.-C. Ren, F. Vollmer, S. Arnold, and A. Libchaber, Opt. Express **15**, 17410 (2007).
10. F. Vollmer, D. Braun, A. Libchaber, M. Khoshsima, I. Teraoka, and S. Arnold, Appl. Phys. Lett. **80**, 4057 (2002).
11. M. A. Santiago-Cordoba, S. V. Boriskina, F. Vollmer, and M. C. Demirel, Appl. Phys. Lett. **99**, 073701 (2011).
12. C.-H. Dong, L. He, Y.-F. Xiao, V. R. Gaddam, S. K. Ozdemir, Z.-F. Han, G.-C. Guo, and L. Yang, Appl. Phys. Lett. **94**, 231119 (2009).
13. M. R. Foreman, F. Sedlmeir, H. G. L. Schwefel, and G. Leuchs, J. Opt. Soc. Am. B **33**, 2177 (2016).
14. F. Ruesink, H. M. Doeleman, R. Hendrikx, A. F. Koenderink, and E. Verhagen, Phys. Rev. Lett. **115**, 203904 (2015).
15. F. Sedlmeir, M. R. Foreman, U. Vogl, R. Zeltner, G. Schunk, D. V. Strekalov, C. Marquardt, G. Leuchs, and H. G. L. Schwefel, Phys. Rev. Appl. **7**, 024029 (2017).
16. D. V. Strekalov, C. Marquardt, A. B. Matsko, H. G. L. Schwefel, and G. Leuchs, J. Opt. **18**, 123002 (2016).
17. F. Sedlmeir, M. Hauer, J. U. Füst, G. Leuchs, and H. G. L. Schwefel, Opt. Express **21**, 23942 (2013).
18. G. Lin, J. Fürst, D. V. Strekalov, I. S. Grudinin, and N. Yu, Opt. Express **20**, 21372 (2012).
19. F. Sedlmeir, R. Zeltner, G. Leuchs, and H. G. L. Schwefel, Opt. Express **22**, 30934 (2014).
20. M. R. Foreman, J. D. Swaim, and F. Vollmer, Adv. Opt. Photon. **7**, 168 (2015).
21. I. Breunig, Laser Photon. Rev. **10**, 569 (2016).
22. T. J. Kippenberg, R. Holzwarth, and S. A. Diddams, Science **332**, 555 (2011).
23. A. Rueda, F. Sedlmeir, M. Kumari, G. Leuchs, and H. G. L. Schwefel, Nature **568**, 378 (2019).
24. G. Lin, A. Coillet, and Y. K. Chembo, Adv. Opt. Photon. **9**, 828 (2017).
25. L. S. Trainor, F. Sedlmeir, C. Peuntinger, and H. G. L. Schwefel, Phys. Rev. Appl. **9**, 024007 (2018).
26. A. Otterpohl, F. Sedlmeir, U. Vogl, T. Dirmeier, G. Shafiee, G. Schunk, D. V. Strekalov, H. G. L. Schwefel, T. Gehring, U. L. Andersen, G. Leuchs, and C. Marquardt, Optica **6**, 1375 (2019).
27. M. Förtsch, T. Gerrits, M. J. Stevens, D. Strekalov, G. Schunk, J. U. Fürst, U. Vogl, F. Sedlmeir, H. G. L. Schwefel, G. Leuchs, S. W. Nam, and C. Marquardt, J. Opt. **17**, 065501 (2015).
28. G. Shafiee, D. V. Strekalov, A. Otterpohl, F. Sedlmeir, G. Schunk, U. Vogl, H. G. L. Schwefel, G. Leuchs, and C. Marquardt, New J. Phys. **22**, 073045 (2020).
29. A. Rueda, F. Sedlmeir, M. C. Collodo, U. Vogl, B. Stiller, G. Schunk, D. V. Strekalov, C. Marquardt, J. M. Fink, O. Painter, G. Leuchs, and H. G. L. Schwefel, Optica **3**, 597 (2016).
30. N. J. Lambert, A. Rueda, F. Sedlmeir, and H. G. L. Schwefel, Adv. Quantum Tech. **3**, 1900077 (2020).
31. W. Hease, A. Rueda, R. Sahu, M. Wulf, G. Arnold, H. G. L. Schwefel, and J. M. Fink, PRX Quantum **1**, 020315 (2020).
32. A. Eschmann and C. W. Gardiner, Phys. Rev. A **49**, 2907 (1994).
33. F. Monifi, Ş. K. Özdemir, and L. Yang, Appl. Phys. Lett. **103**, 181103 (2013).
34. J. Pfeifle, V. Brasch, M. Lauermann, Y. Yu, D. Wegner, T. Herr, K. Hartinger, P. Schindler, J. Li, D. Hillerkuss, R. Schmogrow, C. Weimann, R. Holzwarth, W. Freude, J. Leuthold, T. J. Kippenberg, and C. Koos, Nat. Photonics **8**, 375 (2014).
35. E. Yuce, O. Gurlu, and A. Serpenguzel, IEEE Photon. Technol. Lett. **21**, 1481 (2009).
36. L. He, Ş. K. Özdemir, and L. Yang, Laser Photon. Rev. **7**, 60 (2013).
37. G. Schunk, U. Vogl, D. V. Strekalov, M. Förtsch, F. Sedlmeir, H. G. L. Schwefel, M. Göbelt, S. Christiansen, G. Leuchs, and C. Marquardt, Optica **2**, 773 (2015).
38. J. M. Ward and S. N. Chormaic, Appl. Phys. B **100**, 847 (2010).
39. D. W. Vogt, A. H. Jones, and R. Leonhardt, Appl. Phys. Lett. **113**, 011101 (2018).
40. A. Savchenkov, V. Ilchenko, A. Matsko, and L. Maleki, Electron. Lett. **39**, 389 (2003).
41. V. Ilchenko, P. Volikov, V. Velichansky, F. Treussart, V. Lefèvre-Seguin, J.-M. Raimond, and S. Haroche, Opt. Commun. **145**, 86 (1998).
42. T. Ioppolo and M. V. Ötügen, J. Opt. Soc. Am. B **24**, 2721 (2007).
43. D. W. Vogt, A. H. Jones, H. G. L. Schwefel, and R. Leonhardt, Opt. Lett. **44**, 1319 (2019).
44. D. E. Zelmon, D. L. Small, and D. Jundt, J. Opt. Soc. Am. B **14**, 3319 (1997).
45. H. R. Phillip and E. A. Taft, Phys. Rev. **136**, A1445 (1964).
46. T. Amotchkina, M. Trubetskov, D. Hahner, and V. Pervak, Appl. Opt. **59**, A40 (2020).
47. H. H. Li, J. Phys. Chem. Ref. Data **9**, 561 (1980).
48. D. T. F. Marple, J. Appl. Phys. **35**, 539 (1964).
49. M. Debenham, Appl. Opt. **23**, 2238 (1984).
50. I. H. Malitson and M. J. Dodge, J. Opt. Soc. Am. **62**, 1405 (1972).
51. S. H. Kim, S. H. Lee, J. I. Lim, and K. H. Kim, Appl. Opt. **49**, 910 (2010).
52. G. Ghosh, M. Endo, and T. Iwasaki, J. Lightwave Technol. **12**, 1338 (1994).
53. H. G. L. Schwefel, W. Kähler, Z. H. Lu, J. Fan, and L. J. Wang, Opt. Lett. **33**, 794 (2008).
54. K. Y. Bliokh and A. Aiello, J. Opt. **15**, 014001 (2013).
55. J. Unterhinninghofen, J. Wiersig, and M. Hentschel, Phys. Rev. E **78**, 016201 (2008).
56. Y. A. Demchenko and M. L. Gorodetsky, J. Opt. Soc. Am. B **30**, 3056 (2013).
57. M. Gorodetsky and A. Fomin, IEEE J. Sel. Top. Quantum Electron. **12**, 33 (2006).
58. S. J. Byrnes, "Multilayer optical calculations," arXiv:1603.02720 [physics] (2019).
59. K. G. Cognée, W. Yan, F. L. China, D. Balestri, F. Intonti, M. Gurioli, A. F. Koenderink, and P. Lalanne, Optica **6**, 269 (2019).
60. M. V. Berry, Czech. J. Phys. **54**, 1039 (2004).
61. B. Peng, Ş. K. Özdemir, S. Rotter, H. Yilmaz, M. Liertzer, F. Monifi, C. M. Bender, F. Nori, and L. Yang, Science **346**, 328 (2014).
62. R. El-Ganainy, M. Khajavikhan, D. N. Christodoulides, and Ş. K. Özdemir, Commun. Phys. **2**, 1 (2019).
63. L. Ge and W. Wan, *Emerging Frontiers in Nonlinear Science*, Nonlinear Systems and Complexity, P. G. Kevrekidis, J. Cuevas-Maraver, and A. Saxena, eds. (Springer, 2020), pp. 227–248.